ESF-SILMI – report on the short visit grants refs. 4184 and 4185

Collective stopping power of the fast electron transport in warm dense plasmas

João Jorge Santos[1], Benjamin Vauzour[1], Arnaud Debayle[2] and José Javier Honrubia[2]

[1]*CELIA, Université Bordeaux 1/CNRS/CEA, Talence, France*
[2]*ETSI Aeronáuticos, Universidad Politécnica, Madrid, Spain*

1) Purpose of the visit

J.J. Santos (1st-8th May 2011) and B. Vauzour (2nd-13th May 2011) from CELIA, University of Bordeaux, visited the group of J.J. Honrubia and A. Debayle at the Dpto. Física Aplicada, ETSI Aeronáuticos - Universidad Politécnica de Madrid (UPM). The visit aimed at interpreting the experimental results obtained in 2010 at the LULI2000 laser facility, Ecole Polytechnique, France, by means of numerical simulations.

This experiment had been carried out in the framework of the experimental validation program of the European HiPER project. It is related to the fast ignition (FI) scheme for the energy production in inertial confinement fusion of thermonuclear targets and focuses on the transport a fast electron beam in a dense plasma.

At present time, most of the research work related to fast electron transport was performed with solid density targets at room temperature, at least before fast electron injection. This is of course quite far from the real conditions met in FI, where the density is several times the solid density and with temperatures ranging from around the Fermi temperature to much higher than that. In particular, the target conductivity will be completely different, drastically affecting collective effects in fast electron propagation. The goal of our work is to assess the impact of collective effects in different conditions, but will be also essential to validate, and even to develop, the conductivity models used for warm dense matter at solid or above-solid densities. We want particularly to validate experimentally the models to describe the energy losses of an intense electron beam propagating in dense matter. Such study is of interest not only for fusion but also for astrophysics, and the science of materials in extreme conditions.

2) Experimental work and hydrodynamic modelling carried out before the visit

We studied the fast electron beam (FEB) transport in warm and dense plasmas created from aluminium foils. These were heated to temperatures close to the Fermi temperature and compressed to twice the solid density by shock propagation induced by a long laser pulse (LP beam: $2\omega_0$, 250J, 4.5ns, 0.53μm, $3\text{x}10^{13}$ W/cm^2, 400μm flat-top focal spot). Fast electron beams, generated by a relativistic laser pulse (SP beam: ω_0, 35J, 1.5ps, 1.06μm, 10^{19} W/cm^2, 10μm FWHM focal spot with 25% of the total energy), propagated in the direction opposite to the compressing shock, crossing regions with a wide transversal homogeneity.

Figure 1-a) represents the interaction geometry and the structure of the used multi-layer foil targets. To characterize the FEB transport, we measured the Kα fluorescence yields from tracer layers of different atomic number, embedded at both target extremities to quantify both the fast electron source and the fraction of electrons crossing the target. The used fluorescent layers were 5 μm Ag at the front side and 10 μm Sn plus 10 μm Cu at the rear side.

The SP beam (FEB generation) is delayed with respect to the LP beam. The value of this delay defines the state of the targets at the moment of FEB generation. It was previously predicted by 2D axis-symmetric radiative-hydrodynamic simulations performed with the code

CHIC[1], describing both the LP beam interaction at the rear side and consequent shock generation and propagation through the target as well as the 1.1 ns, ~10^{12} W/cm^2 amplified spontaneous emission (ASE) pedestal of the SP beam. Figures 1-b) and c) show the density, ionization degree and temperature profiles of a 20 µm-propagation layer target for the two tested SP beam injection times: panel b) corresponds to a short SP/LP delay where the LP-induced shock has just crossed the rear side tracer-layers and not yet reached the Al-propagation layer: In this case the FEB propagates in a solid density and initial cold target and the coronal plasma created by the LP beam at the target rear works as a *get lost layer* which traps the fast electrons having crossed the target and inhibits their recirculation. Panel c) corresponds to the same target but when the Al-propagation layer is almost entirely compressed: in this case the fast electrons cross a propagation layer where, exception to the first 3 to 4 µm, the density has been raised by a factor two and the material is heated to 2-3 eV, close to Fermi temperature. When varying the propagation layer thickness, the SP/LP delay was always kept constant for the shots in solid propagation-layer targets (situation depicted in Fig. 1-b). For the shots on compressed propagation-layer targets, the SP/LP delay was adjusted accordingly to the target thickness and to CHIC hydrodynamic predictions, in order to prevent any front side Ag-tracer alteration by the compressing shock. The hydrodynamic simulations were benchmarked at the beginning of the experiment by Streaked-Optical-Pyrometry (SOP) measurements of the shock breakthrough at the propagation-layer front surface (using special targets without the Al-generation and Ag-front tracer layers).

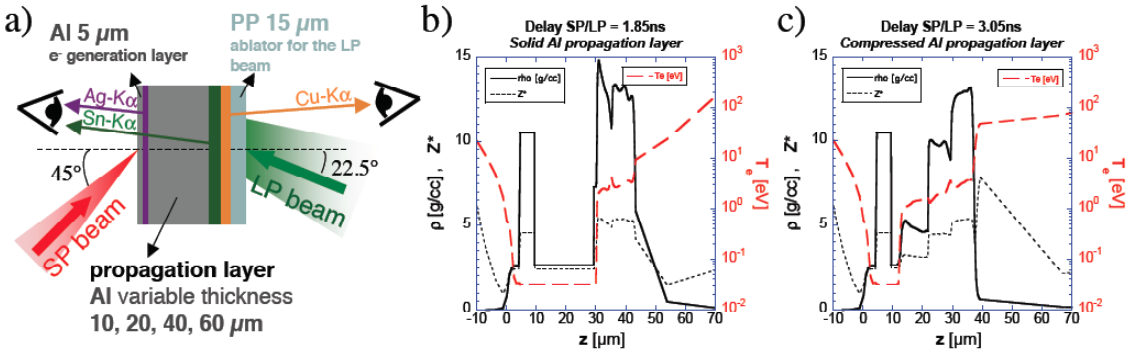

Figure 1: a) Sketch of the multi-layer target structure and of the LP and SP laser beams interaction geometry. On the right, the density (full black curves), ionization degree (dotted black curves) and electron temperature (red dashed curves) profiles of either **b)** solid or **c)** compressed 20 µm-propagation-layer targets.

The Cu-Kα signals were imaged with a spherical quartz crystal: the signal diameter (full-with at half-maximum, FWHM) as a function of the Al-propagation layer thickness (accounting for its compression) is shown in Figure 2-a) (full symbols). The Ag- and Sn-Kα yields were measured with an absolute calibrated Cauchois-type X-ray transmission spectrometer and are respectively shown in Figure 2-b) and c) (full symbols).

3) Fast electron transport simulation work carried out during the visit

The work carried out in Madrid in the framework of these ESF grants was devoted to reproduce the experience via simulations of the fast electron transport. We performed 2D axisymmetric hybrid simulations[2] using the density and temperature profiles predicted by the hydrodynamic code CHIC. The FEB energy and angular distributions input to the hybrid code were initially estimated from a 2D collisionless particle-in-cell (PIC) simulation using the code CALDER[3], and then slightly and progressively readjusted to reproduce the better possible the experimental measurements of the Cu-Kα emission spot diameter and Ag- and Sn-Kα yields.

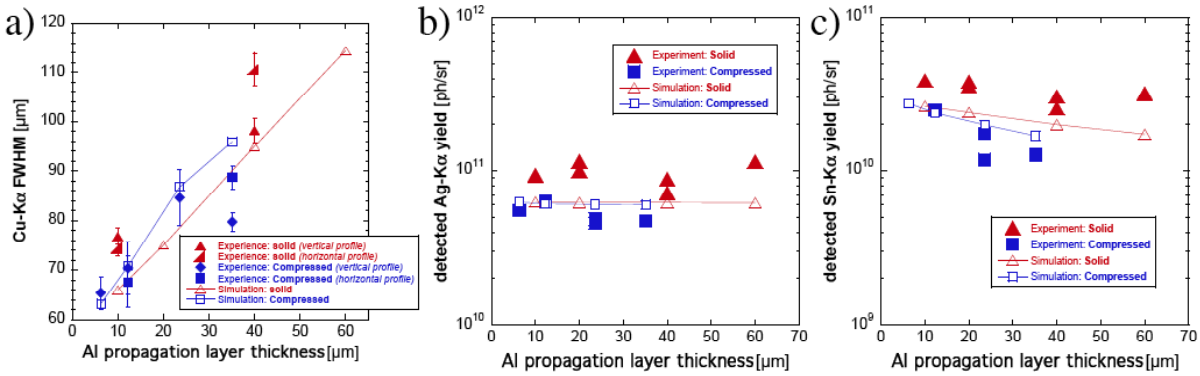

Figure 2: a) Cu-Kα diameter (FWHM), **b)** Ag- and **c)** Sn-Kα detected yields against the thickness of the Al-propagation layer, for solid (red symbols) and compressed (blue symbols) targets. The experimental data (full symbols) are compared to results from hybrid fast electron transport simulations (open symbols).

The hybrid transport simulation results are plotted in Fig. 2 (open symbols) and compared to the experimental data (full symbols). After a few iterations, the electron source input parameters were optimized as follows:

i. Angular distribution defined by the model function[4] $f(\theta)=\exp[-(\theta-\theta_r \arctan(r/r_0))^2/\Delta\theta_0^2]$, with the dispersion angle $\Delta\theta_0=55°$ and the mean radial angle $\theta_r=30°$.

ii. The electron beam injection radius $r_0=20\ \mu$m, which is about twice the radius of the SP laser spot containing half of the on-target laser energy. This is coherent with a laser halo energy dispersion around the focal spot, as observed during the experiment.

iii. The low-energy component (0.008 to 2 MeV) of the electron energy distribution was approximated to a decreasing exponential with a mean energy 220 keV. The time-integrated energy flux through the injection surface carries 40% of the time-integrated laser energy.

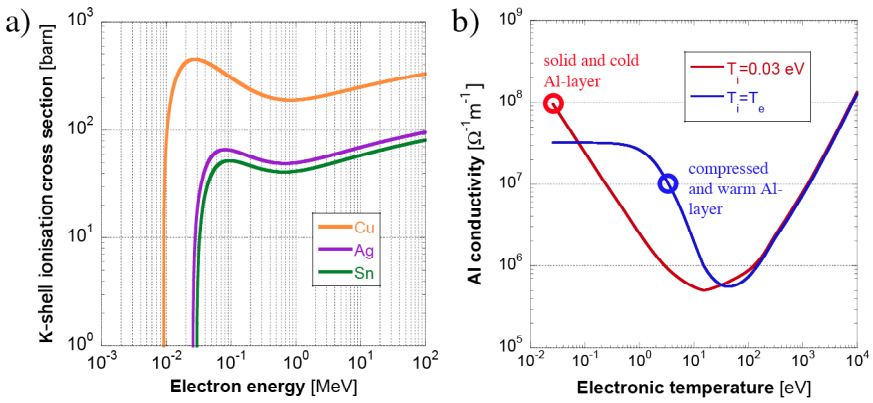

Figure 3: a) K-shell ionisation cross sections by impact of an electron against its energy for the used Kα tracer materials. **b)** Electrical conductivity of aluminium against the electronic temperature for a cold ion population (red curve) and a plasma at thermodynamic equilibrium (blue curve). The initial conductivity values (before FEB injection) estimated for our experimental conditions are pointed out for solid (red symbol) and compressed (blue symbol) Al-propagation layers.

More details on the hybrid transport, as the ionization model, can be found in Ref. 1, but we point here that the Kα emission from the tracer layers was calculated on-the-fly from the cross sections derived in Ref. 5 and plotted in Fig. 3-a). The electrical conductivity of the metallic layers was computed using the classical Drude model, $\sigma = e^2 n_e / m_e \nu$, where e is the

elementary charge, n_e the background electron density, m_e the electron rest mass, and ν the collision frequency expressed as a harmonic mean between electron-phonon, electron-electron, collision saturation and Spitzer collision frequencies[6]: As an example, the electrical conductivity of aluminium is plotted in Fig. 3-b) against the electronic temperature for a cold ion population (red curve) and a plasma at thermodynamic equilibrium, T_e=T_i (blue curve).

Once we correctly tuned the FEB source in order to reproduce the experimental data, we investigated via the simulations the way the FEB loses its energy while propagating in the compressed Al-propagation layer and compared it to the solid case. Figure 4-a) shows the ratio of target rear-side fluorescence yield over front-side fluorescence yield, Sn-Kα/Ag-Kα. It roughly represents the fraction of the generated fast electrons with energies > 75 keV that reaches the Sn tracer located after the Al-propagation layer, as a function of its thickness. We can appreciate the good agreement between experimental data (full symbols) and the results of the hybrid electron transport simulations (open symbols). The fluorescence ratio decreases with the thickness of the Al-propagation layer but with a more important rate in the case of the compressed targets.

Very basically, we can consider two principal mechanisms for the FEB energy losses:

i. Fast electrons loose energy via their direct collisions with the background material. In principle, the integrated collisional energy loss is proportional to the mean propagation layer areal density:

$$\left.\frac{dE}{dz}\right|_{collisions} \propto \rho \quad \Rightarrow \quad \Delta E|_{collisions} \propto \langle \rho \rangle L_{Al} \qquad (1)$$

We have obtained a density compression factor $\rho_{compressed}/\rho_{solid} \approx 2$ (Fig. 1-b) and c)).

ii. Fast electrons also loose energy because of the target resistivity. The integrated energy loss is inversely proportional to the background material conductivity σ:

$$\left.\frac{dE}{dz}\right|_{resistive} = e\frac{j_h}{\sigma} \quad \Rightarrow \quad \Delta E|_{resistive} \propto \left\langle \frac{j_h}{\sigma} \right\rangle L_{Al} \qquad (2)$$

According to our conductivity model, $\sigma_{compressed}/\sigma_{solid} \approx 1/10$ (see Fig. 3-b)).

In the equations, dE/dz is the electron energy loss spatial rate, j_h the FEB current density, L_{Al} the thickness of the Al-propagation layer as seen by the FEB (according to the compression). The brackets <…> stand for the means over the length of this layer.

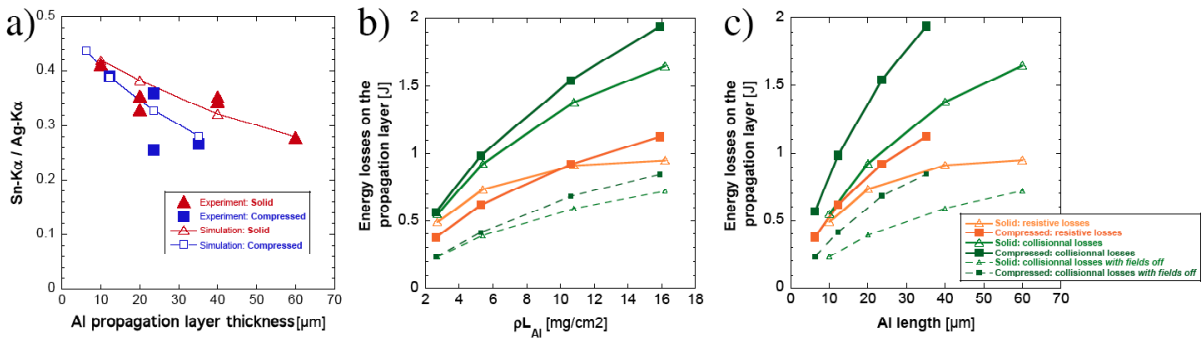

Figure 4: a) Experimental (full symbols) and simulated (open symbols) of the target rear-side-fluorescence yield (Sn-Kα) over the front-side-fluorescence yield (Ag-Kα) against the Al-propagation layer thickness. **b)** and **c)** FEB energy losses integrated over the thickness of solid (open triangles) and compressed Al-propagation layers (solid squares) against its **a)** areal density and **b)** thickness. Orange symbols correspond to the resistive losses, and green symbols to collisional losses. Smaller green symbols (connected by dashed lines) correspond to electron transport simulations without electromagnetic fields using the same FEB source parameters.

The energy losses integrated over the Al-propagation layer resulting from the hybrid transport simulations are plotted in Figure 4 as a function of b) the areal density and c) the thickness of the Al-propagation layer. Orange symbols correspond to the resistive losses, $\Delta E\big|_{resistive}$, and green symbols to collisional losses, $\Delta E\big|_{collisional}$. Smaller green symbols (connected by dashed lines) correspond to transport simulations without electromagnetic fields using the same FEB source parameters: in this case the total energy losses are strictly due to the collisions of the FEB with the background material.

In a planar compression, the areal density along the electrons propagation axis is not significantly varied upon compression. Therefore and according to (1), we expected to not observe any change in the integrated collisional energy losses upon compression. But as one can see in Fig. 4-b), this is not exactly the case: when comparing results for identical initial targets, we see the collisional losses difference between the results for compressed and for solid Al layers to rise with the areal density. This is even more pronounced in the simulation with a full physical description, including collisions and self-generated fields (green points connected by full lines), than in the case when the fields are turned off in the simulation (smaller green points connected by dashed lines).

Looking to the integrated energy losses against the thickness of the Al-propagation layer in Fig. 4-b), we can qualitatively conclude that:

i. Both collisional and resistive energy loss mechanisms are stronger in compressed targets, respectively in agreement with a rise of the Al-propagation layer density and the diminution of its conductivity.

ii. FEB collisional energy losses are preponderant, but resistive losses are not at all negligible (both in solid and compressed matter), as naively supposed in many integrated simulations of FI targets published in literature.

iii. Actually, by turning off the effects of the fields self-generated by the injected intense fast electron current, the collisional losses become less important than the collective losses. In a full description, resistive effects considerably slow down the FEB and contribute indirectly to enhance the collisional stopping. The resistive stopping being more important in compressed matter, these also enhance the difference between the collisional losses in compressed compared to solid Al for targets of the same areal density.

4) Preliminary conclusions and future collaboration with the host institution

This experience has enabled us to confirm that the electron transport is more dissipative in the compressed aluminium, compared to solid density aluminium. The enhanced dissipation of energy is not only due to the fast electrons collisions with the background material. Indeed, the resistive effects play an important dissipative role, mainly on the transport of low energy electrons to which the Kα emission is particularly sensible.

We are carrying out further electron transport simulations through a distant connection to the UPM servers. We are presently analysing the scaling of the fast electron beam divergence and of the energy loss mechanisms in solid matter and in warm dense plasma for incident electron current densities in the range from 10^{10} to 10^{12} A/cm^2.

The observed phenomena will to be confirmed in a near future experiment broadening the regime of the tested laser intensities up to 2 10^{20} W/cm^2. The experiment will be carried out by the CELIA group in July-August 2011 at the Titan laser facility at the Lawrence Livermore National Laboratory, USA. We expect to generate FEB with current densities up to a few

10^{13} A/cm^2. We will certainly continue the fructuous collaboration with the UPM group for the interpretation of the future experimental data.

5) Projected communications at international conferences and publications

The ensemble of experimental and simulation results will be presented at the forthcoming 7th Inertial Fusion Sciences and Applications (IFSA) conference to be held in Bordeaux in September 2011. It will also be object of an article submission to a peer-reviewed journal.

These will include a precise quantitative analysis of the effects identified above on the FEB stopping mechanisms upon matter compression and heating to temperatures close to Fermi temperature. A scaling on the FEB current density and extrapolation to a real-size FI scenario, in terms of injected FEB current density and of background plasma density, temperature and conductivity, will also be discussed.

Made in Talence, France, the 8th June 2011

João Jorge Santos

Benjamin Vauzour

[1] P. H. Maire, R. Abgrall, J. Breil, and J. Ovadia, SIAM J. Sci. Comput. **29**(4), 1781 (2007). P. H. Maire and J. Breil, Int. J. Numer. Methods Fluids **56**, 1161 (2008).
[2] J. J. Honrubia *et al*., Phys. Plasmas **12**, 052708 (2005).
[3] E. Lefebvre *et al*., Nuclear Fusion **43**, 629 (2003).
[4] A. Debayle *et al*., Phys. Rev. E **82**, 036405 (2010).
[5] C. Hombourger, J. Phys. B: At. Mol. Opt. Phys. **31**, 3693 (1998).
[6] B. Chimier *et al*., Phys. Rev. B **75**, 195124 (2007).